FULL PAPER

Kinetic Monte Carlo Study of the Sensitivity of OLED Efficiency and Lifetime to Materials Parameters

Reinder Coehoorn, Harm van Eersel, Peter A. Bobbert, and René A. J. Janssen*

The performance of organic light-emitting diodes (OLEDs) is determined by a complex interplay of the optoelectronic processes in the active layer stack. In order to enable simulation-assisted layer stack development, a three-dimensional kinetic Monte Carlo OLED simulation method which includes the charge transport and all excitonic processes is developed. In this paper, the results are presented of simulations including degradation processes in idealized but realizable phosphorescent OLEDs. Degradation is treated as a result of the conversion of emitter molecules to non-emissive sites upon a triplet-polaron quenching (TPQ) process. Under the assumptions made, TPQ provides the dominant contribution to the roll-off. There is therefore a strong relationship between the roll-off and the lifetime. This is quantified using a "uniform density model", within which the charge carrier and exciton densities are assumed to be uniform across the emissive layer. The simulations give rise to design rules regarding the energy levels, and are used to study the sensitivity of the roll-off and lifetime to various other materials parameters, including the mobility, the phosphorescent dye concentration, the triplet exciton emissive lifetime and binding energy, and the type of TPQ process.

1. Introduction

Organic light-emitting diode (OLED) technology for large area lighting is presently developing from design-focused special-lighting applications towards general-lighting applications for homes and offices. Future products are expected to show added functionality such as flexibility, transparency in the off-state, and color-tunability. Continuous improvements of the system power efficiency and long-term stability arise from the use of novel organic semiconductor materials, novel stack architectures and methods for improved light outcoupling.[1]

The development of OLED active layer stacks is supported by the use of simulation methods. As indicated schematically in **Figure 1**, two types of applications may be distinguished: i) revealing the mechanism of the relevant charge transport and excitonic processes and determining the values of the relevant material-specific parameters, ii) supporting the layer stack design process by providing an efficient route for developing understanding of the benefits and disadvantages of the use of novel materials and layer stack concepts. The third (vertical) axis in the figure indicates examples of the performance characteristics which may be studied using the simulations. We envisage that simulations can be used to clarify the sensitivity of the OLED device performance to materials and layer stack parameters, and can provide insights in the functioning of OLEDs beyond the capability of experiments. For example by a much more precise control of the device structure, by providing insight in all processes at an ultimate (molecular-scale) spatial resolution and at the shortest relevant time scales, and by providing the opportunity to explore the performance under conditions which are experimentally not realizable. A long-term goal of our research is therefore to develop and apply a simulation method which can address any combination of the three application types, and which provides a platform within which novel insights as obtained in each of the fields indicated in the figure can be readily adopted.

So far, commonly used OLED simulations methods are based on one-dimensional drift-diffusion approaches (see Coehoorn and Bobbert and references therein)[2] in which the charge transport and excitonic processes are included in a semi-empirical manner. However, it is well-known that as a result of the energetic disorder, resulting from the structural disorder, the current density in OLEDs is filamentary, rather than uniform.[3] We have shown from molecular-scale three-dimensional kinetic Monte Carlo (3D-KMC) modelling that, as a consequence, the emission takes place on certain preferred molecular sites, rather than being laterally uniform.[4] It is thus necessary to develop a full 3D-KMC model for accurately simulating the effect of the loss processes, such as triplet-polaron quenching and triplet-triplet annihilation in phosphorescent OLEDs. These losses lead to an efficiency decrease with increasing current density and luminance (roll-off of the internal quantum efficiency, η_{IQE}). We have recently extended the 3D-KMC method to include the charge transport and all excitonic processes in an integral manner.[5] The simulations were found to provide a good description of the roll-off of archetypical green and red emitting OLEDs studied intensively in the literature,[6] and were used to

Prof. R. Coehoorn, H. van Eersel
Philips Research Laboratories
High Tech Campus 4, 5656AE, Eindhoven
The Netherlands
E-mail: reinder.coehoorn@philips.com
Prof. R. Coehoorn, H. van Eersel,
Dr. P. A. Bobbert, Prof. R. A. J. Janssen
Department of Applied Physics
Eindhoven University of Technology, P.O. Box 513
5600MB, Eindhoven, The Netherlands

DOI: 10.1002/adfm.201402532

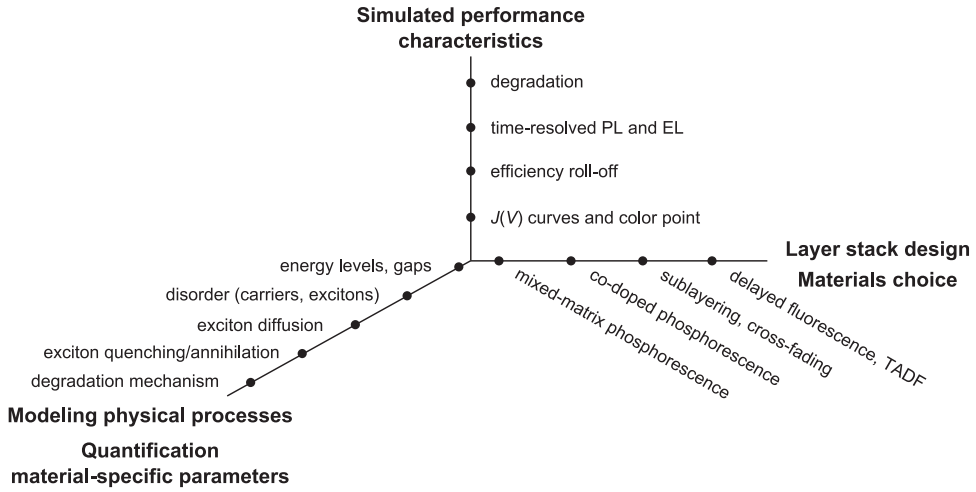

Figure 1. Application areas of OLED device simulations (horizontal and diagonal axes) and examples of the performance characteristics which may be studied (vertical axis). TADF denotes Thermally Assisted Delayed Fluorescence.[7,8] Simulation studies for a variety of performance characteristics, layer stack designs and materials can help to develop an improved material-specific understanding of the relevant physical processes. Realizing progress in that understanding is needed to make simulation-assisted OLED stack development more powerful.

develop a design rule for an optimal power efficiency, resulting from a small η_{IQE}-roll-off and a low voltage.

In this paper, we demonstrate how 3D-KMC simulations can also be used to predict the dependence of the lifetime of phosphorescent OLEDs on the materials and layer stack parameters. For that purpose, we have included in the simulations irreversible changes of the molecular sites, according to a chosen scenario, and simulate the resulting time-dependence of the emission. Whereas a wide variety of degradation mechanisms can be operative,[7,8] recent work has indicated that in phosphorescent OLEDs triplet-polaron quenching followed by defect formation can play a major role.[9,10] We investigate two degradation scenarios in which upon triplet-polaron quenching the dye molecule which is involved is with a certain probability converted in a non-emissive molecule. These explicit 3D-KMC lifetime simulations can be computationally intensive. We have therefore also studied to what extent it is already possible to predict lifetime trends using the loss due to exciton-polaron quenching as obtained from results of the steady-state simulations. As a first step towards that goal, we focus on the case of monochrome OLEDs with a single emissive layer (EML), and show how under the simplifying assumption that the charge carrier density and exciton generation are uniform across the thickness of the EML the roll-off can be expressed in terms of the materials and layer stack parameters. The approach is a refinement of earlier work,[11,12] by including the charge carrier density dependence of the mobility and by including a mechanistic expression for the triplet-polaron quenching rate. As a second step, it is shown how using this uniform density model (UDM) variations of the lifetime with layer stack parameters, such as the EML thickness or dye concentration, can then be predicted from the roll-off. Within the degradation scenarios considered, the absolute lifetime is proportional to the inverse of the probability that upon a quenching event degradation takes place. That is the only additional parameter which is required. Within the framework of our approach, it can be determined by one or a few "calibration" experiments. We stress that the UDM only provides a starting point for analyses of roll-off and lifetime. The simulations show that changes of the shape of the charge carrier density and emission profiles with the voltage and current density also play an important role.

The paper is organized as follows. Section 2 contains an overview of the simulation method and a simulation example. In Section 3, the uniform density model is developed, and analytical expressions are given for the dependence of the roll-off and lifetime on the material parameters, neglecting exciton dissociation and exciton diffusion. In Sections 4 and 5, the sensitivity of the roll-off and lifetime, respectively, to various materials parameters is studied from 3D-KMC simulations. Two design rules for the most optimal energy level structures are established, and the sensitivity of the roll-off to the emissive lifetime of the dye molecules and to the triplet binding energy is examined. The UDM is shown to provide a fair prediction of the OLED lifetime for small dye concentrations, for which exciton diffusion to already degraded sites may be neglected. Section 6 contains a summary, conclusions and outlook.

2. Simulation Method

In this section, firstly an overview is given of the 3D-KMC simulation method and of the simulation parameters used in this paper (subsection 2.1). Subsequently, more detailed descriptions are given on the treatment of charge transport, excitonic processes and degradation (subsections 2.2, 2.3 and 2.4, respectively). Finally, as an example the simulations are applied in subsection 2.5 to a symmetric three-layer OLED, for which the roll-off curve, emission profile, carrier density profile and time-dependent decrease of the emission due to degradation is shown. In Section 4, the energy level structure assumed for this example will be shown to quite optimally fulfill two design rules leading to a small roll-off, and in Section 5, the sensitivity

of the OLED lifetime when varying the Ir-dye concentration in this OLED will be discussed.

2.1. Simulation Parameters—Overview

Within the 3D-KMC simulation method developed, the molecules are treated as point sites, without any internal structure. The sites are placed on a simple cubic grid with a lattice parameter $a = N_t^{-1/3}$, with N_t the average molecular site density. Any layer sequence and mixing of different types of molecules in each layer can be defined, such as random mixing, aggregation of similar molecules,[13] mixed interface layers, or, for example, a concentration gradient in the emissive layer.[14,15] At any moment in time, a site in the box is either empty, or occupied by one electron, one hole, or by one electron and one hole. When at a site a compound species (exciton, one electron and one hole) is present, the exciton is further specified as either a singlet or a triplet exciton. Typically, for each set of external conditions (voltage, temperature) five parallel simulations are carried out for nominally equal boxes, but with different disorder realizations, with a lateral area of 50×50 sites. From the time-resolved and time-averaged results as obtained for these simulation boxes, the statistical uncertainty can be judged.

The simulations are specified by four sets of parameters: i) parameters defining the system structure (thicknesses and composition of all sub-layers), ii) electrical parameters, iii) excitonic parameters, iv) the parameters specifying the external conditions (voltage, V, and temperature, T). The charge transport and excitonic processes are included in a manner as described by Mesta et al.[4] and by van Eersel et al.[5] A brief description is given in the next subsections. **Table 1** gives an overview of the basic electrical and excitonic parameters, and their values used as a default in the simulations discussed in this paper. We note that the code allows for various refinements, not mentioned further here, such as non-isotropic mobilities, non-Gaussian shapes of the density of states, and long-distance (e.g., Förster-type) exciton-polaron quenching and exciton-exciton annihilation. Furthermore, it allows for carrying out simulations under special conditions, such as steady-state or time-resolved photoluminescence[11,16,17] or electroluminescence conditions.[18] All simulations were done for $T = 298$ K.

Table 1. Overview of the electrical and excitonic parameters used in the 3D-KMC simulations, and the default values used in this paper.

Parameter	Description	Value
ν_1	Hopping attempt rate to the first neighbor	3.3×10^{10} s^{-1}
σ	Width (standard deviation) of the Gaussian density of states	0.10 eV
N_t	Site density	10^{27} m^{-3}
λ	Wavefunction decay length	0.3 nm
ε_r	Relative dielectric constant	3.0
$E_{T,b}$	Triplet exciton binding energy	1.0 eV
$k_{D,0}$	Dexter transfer prefactor	1.6×10^{-10} s^{-1}
$R_{F,diff}$	Förster radius for exciton diffusion between dye molecules	1.5 nm
Γ_{rad}	Radiative decay rate dye molecules[a)]	0.544 μs^{-1}
Γ_{nr}	Non-radiative decay rate dye molecules[a)]	0.181 μs^{-1}

[a)]Values as obtained experimentally for the orange-red emitter $Ir(MDQ)_2(acac)$ in an α-NPD matrix, assuming a radiative decay efficiency $\eta_{rad} = 0.75$, intermediate between the values obtained from analyses assuming randomly oriented or mainly parallel emission dipole moments.[19]

The accessible material and device parameter range is determined by practical (real time, CPU time, memory) limitations. The total required real simulation time depends on the level of time-averaged, spatially resolved or time-resolved detail needed and the number of nominally equal OLEDs with different disorder realizations run in parallel. When considering five 50 nm × 50 nm of such OLEDs in parallel, the IQE roll-off curve simulations discussed in this paper are obtained typically in 3–10 days on a 3.0 GHz core [Intel Xeon X5675], depending on the current density. Simulations in which the fraction of quenched excitons or the fraction of radiatively decaying excitons is small (at a very small current or very large current density, respectively) are most demanding, since a large number of events needs to be recorded to gather enough statistics on the most rare event. The lifetime results discussed in this paper are based on simulations over periods ranging from a few days up to two months. Achieving sufficient statistics is slowed down when considering larger device dimensions, larger energy barriers at interfaces, enlarged charge carrier or exciton hop distances (due to enlarged wavefunction decay lengths or Förster radii, at large fields, or in very dilute systems), enlarged density of states widths or trap depths, and enlarged exciton lifetimes (so that at a given time more excitons are present in the device).

2.2. Charge Transport

The hop rate ν of electrons and holes over a distance R and from a molecule with energy E_i (initial state energy) to a molecule with $E_f = E_i + \Delta E$ (final state energy) is assumed to be given by the Miller-Abrahams formalism. When the hopping occurs between two molecules of types A and B the rate is assumed to be given by:

$$\nu = \sqrt{\nu_{1,A}\nu_{1,B}}\exp\left[-2\alpha(R-a)\right]\exp\left(-\frac{|\Delta E|-\Delta E}{2k_BT}\right) \quad (1)$$

where $\nu_{1,X}$ is the hopping attempt rate between two molecules of type X at a distance a (first neighbor), for the case $\Delta E = 0$, and $\alpha \equiv 1/\lambda$ is the inverse of the wavefunction decay length (λ). The square-root form of the prefactor used arises when considering the transfer integral due to the overlap of the two exponentially decaying wavefunctions. The expression applies to any pair of molecules, also to molecules in different layers. So no special parameters are introduced to describe the hop rates across internal interfaces. In this paper, materials with spatially uncorrelated Gaussian disorder are considered. The hole and electron site energies are taken from a random Gaussian distribution with a material-specific mean value and with a material-specific standard deviation σ_h or σ_e, respectively, modified by i) the Coulomb interaction energy with the other

charge-carriers and with its image charges in the electrodes and by ii) the electrostatic potential difference due to the field arising from the applied voltage. As in the transport processes studied holes or electrons are removed or added, the material-specific mean energy level values for holes and electrons should be termed properly as a mean ionization potential or a mean electron affinity, respectively. However, we indicate these energies instead as a highest occupied molecular orbital (HOMO) energy, E_{HOMO}, or a lowest unoccupied molecular orbital (LUMO) energy, E_{LUMO}, respectively, as is common practice in the literature.

By using this mechanistic approach, we circumvent the need to describe the charge transport by means of complicated expressions for the mobility and diffusion coefficient, which are used in one-dimensional drift-diffusion simulations. The mobility, e.g., depends on the charge carrier density, electric field and temperature, and is affected by the shape of the density of states, the type of disorder, Coulomb interaction effects in accumulation regions near interfaces, and the presence of guest or trap molecules.[2] Furthermore, the mobility may effectively be time (or frequency) dependent due to charge carrier relaxation[20,21] and it is effectively layer thickness dependent below a certain critical length scale.[22]

In a uniform layer, the mobility at any field, temperature and carrier density is determined by four material parameters: a, σ, ν_1 and λ. These parameters can be determined from dedicated transport studies of single-carrier single-layer devices, as shown for several polymeric[23–25] and small-molecule materials.[26,27] The lattice parameter a which is obtained from such studies, is quite similar to the value expected from the experimental molecular site density. In this paper, we take $a = 1$ nm, $\sigma = 0.1$ eV, and $\nu_1 = 3.3 \times 10^{10}$ s^{-1}, which are typical values for small-molecule OLED materials (see van Eersel et al.[5] for a motivation of the choice for ν_1). The wavefunction decay length λ is only relevant in dilute host-guest systems in which guest-guest hopping over distances larger than a is significant. From such studies, we deduce that λ is larger than the value of $0.1 \times a$ (i.e., 0.1 nm for $a = 1$ nm) which has been used in earlier modeling studies of transport in one-component materials.[4,28,29] In this paper, we take $\lambda = 0.3$ nm, the value used by van Eersel et al. to describe the roll-off in Ir(ppy)$_3$ and PtOEP based OLEDs.[5] Within a more refined approach, the hop rates should be described using Marcus theory.[30] However, as an additional parameter would be involved (the reorganization energy), to which the shape of the current voltage-curves will be quite insensitive,[31] we have not adopted that approach. Based on similar arguments (see also Cottaar et al.),[31] a simple cubic grid is used in all cases instead of treating the grid structure as a degree of freedom.

2.3. Excitonic Processes

Exciton generation (dissociation) is treated as a result of a hop of a charge carrier to (away from) a site at which already a carrier of the opposite polarity resides, using Equation (1), albeit that ΔE includes now a gain (loss) equal to the on-site singlet or triplet exciton binding energy, $E_{\mathrm{S(T),b}}$. This takes into account that the actual on-site exciton binding energy is finite, whereas within the point-site model used the on-site electron-hole Coulomb interaction would be infinite. In this paper, we focus on phosphorescent OLEDs and take the triplet binding energy equal for all sites. Exciton generation and dissociation are thus a natural consequence of the electron-hole attraction; no additional rate coefficients are introduced. The Coulomb interaction energy between an electron and hole on a nearest neighbor site (a charge-transfer exciton) is within our formalism equal to $E_{\mathrm{CT,b}} = e/(4\pi\varepsilon_0\varepsilon_r a)$, with e the electron charge, ε_0 the vacuum permittivity and ε_r the relative dielectric constant (taken equal to 3), that is, 0.48 eV. In a homogeneous material, a significant dissociation rate will thus be obtained unless the exciton binding energy is well above $E_{\mathrm{CT,b}}$. In Section 4, we study the sensitivity of the roll-off to $E_{\mathrm{T,b}}$. In this paper, we assume that all excitons which are generated are triplets. As we consider only devices in which almost all the excitons are formed on the phosphorescent dye molecules, so that singlet-to-triplet conversion due to intersystem crossing is fast, that is an excellent approximation.

Radiative and non-radiative decay are assumed to be mono-exponential processes with rates Γ_{rad} and Γ_{nr}, respectively, which may be deduced from the measured total decay rate $\Gamma = \Gamma_{\mathrm{rad}} + \Gamma_{\mathrm{nr}} \equiv \tau^{-1}$ (with τ the effective decay time) and the radiative decay efficiency η_{rad} (which may be taken equal to the photoluminescence efficiency) using the expressions $\Gamma_{\mathrm{rad}} = \eta_{\mathrm{rad}}\Gamma$ and $\Gamma_{\mathrm{nr}} = (1 - \eta_{\mathrm{rad}})\Gamma$.

The exciton transfer rate from a site of type A to a site of type B, at a distance R, is described as a sum of contributions due to Förster transfer, with a rate

$$k_{\mathrm{F,AB}} = \Gamma\left(\frac{R_{\mathrm{F,diff,AB}}}{R}\right)^6 \tag{2}$$

with $R_{\mathrm{F,diff,AB}}$ the Förster radius for exciton diffusion between the two types (A, B) of molecules involved, and a Dexter contribution given by

$$k_{\mathrm{D}} = \sqrt{k_{\mathrm{D,0A}}k_{\mathrm{D,0B}}}\exp[-2\alpha R]\exp\left(-\frac{\Delta E + |\Delta E|}{2k_{\mathrm{B}}T}\right) \tag{3}$$

where $k_{\mathrm{D,0,A(B)}}$ are material-type specific prefactors, α is the inverse of the wavefunction decay length, and ΔE is the difference between the final and initial state exciton energies. Such an energy difference can occur when the two molecule types are different, or as a result of excitonic disorder. In this paper, excitonic disorder is neglected. Only few studies on triplet exciton diffusion in phosphorescent host-guest systems have been carried out. Based on the work of Kawamura et al.,[32] we take $R_{\mathrm{F,diff}} = 1.5$ nm. It has also been argued that exciton diffusion between Ir-dye molecules is predominantly due to Dexter transfer.[33,34] In view of this uncertainty, we take the Dexter prefactors such that at a distance equal to the Förster radius both rates are approximately equal. At much larger distances the diffusion is then predominantly due to the Förster process, whereas at distances of 1–2 nm also Dexter transfer contributes.

The detailed mechanisms of triplet-polaron quenching (TPQ) and triplet-triplet annihilation (TTA) are not well known. In this paper, we describe both processes as immediate when the two interacting species are at a distance a. A distinction

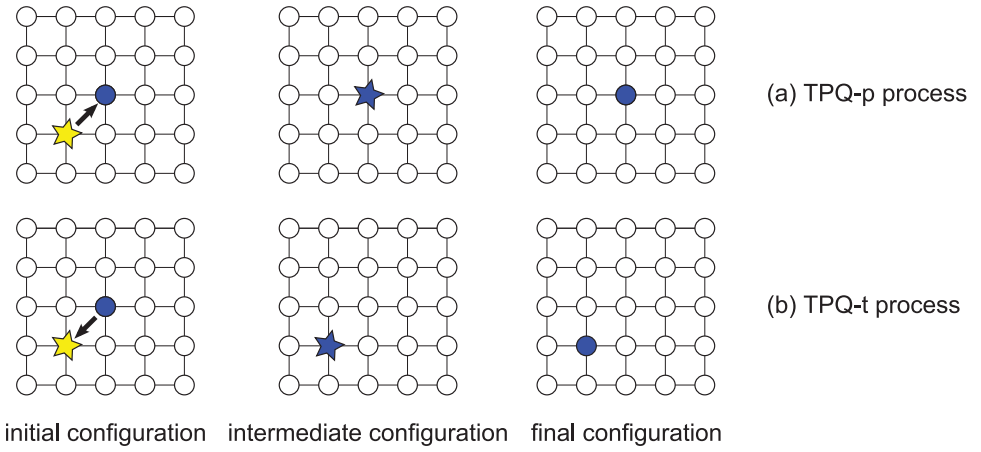

Figure 2. The two types of triplet-polaron quenching processes considered: a) TPQ-p process, and b) TPQ-t process. Empty circles: neutral molecules in the ground states. Filled circles: molecules on which a polaron resides, in the polaronic ground state. Stars (initial configuration): neutral molecules in the lowest triplet exciton state. Stars (intermediate configuration): polaron in an excited state.

is made between TPQ processes in which the triplet is transferred to the site at which the polaron resides ("TPQ-p process") or one in which the polaron hops to the site at which the triplet resides ("TPQ-t process") (see **Figure 2**). Making this distinction does not affect the roll-off. However, it can affect the degradation rate (see Section 5). After a TTA process one triplet exciton is assumed to be left, randomly chosen to be on one of the dye sites. Under these assumptions, no free parameters describing TPQ and TTA are introduced. The TPQ rate is then determined predominantly by the polaron density and the polaron diffusion coefficient (see the next section), as for the dilute systems considered the triplet diffusion coefficient is relatively small. The TTA rate is at the low voltages considered for lighting applications very small, in view of the small triplet volume density obtained for the commonly used short radiative lifetime phosphorescent Ir-based emitters, and the small triplet diffusion coefficient.[5] In a forthcoming paper, we investigate to what extent TPQ still provides the dominant contribution to the roll-off when describing TPQ and TTA as long-range Förster-type processes with Förster radii up to 5 nm,[35] as suggested, for instance, for the case of TTA from the work of Reineke et al.[16]

2.4. Degradation

In this paper, we describe OLED degradation as a result of the conversion of emitter sites to non-emissive sites with an infinite value of Γ_{nr} when on that site a TPQ process occurs, with a probability p_{degr}. All other parameters are kept constant. The effect of degradation is only included when mentioned explicitly. In such a case, we first carry out a steady-state 3D-KMC simulation without degradation ($p_{degr} = 0$), in order to obtain equilibrated charge and exciton distributions. Subsequently, we continue the simulation under the condition $p_{degr} = 1$. Our approach thus employs the largest possible acceleration, in order to make the simulations feasible. We find that such an approach is permitted, as simulations using a smaller value of p_{degr} lead to a decrease of the decay rate which is proportional to p_{degr}. We remark that p_{degr} is in reality expected to be a very small number. The decay of the emission intensity is found to show in general a stretched-exponential-like shape, as is also observed experimentally. The lifetime is shorter for the case of TPQ at the site where the triplet resides (TPQ-t) than for the case of TPQ at the site where the polaron resides (TPQ-p), as only in the former case all TPQ processes occur on an emitter molecule (see Section 5).

2.5. Example: Mixed Matrix Symmetric OLED

As a first example, we discuss the results of 3D-KMC simulations for a symmetric OLED with a layer structure (anode | HTL (40 nm) | EML (20 nm) | ETL (40 nm) | cathode), with a mixed-matrix emissive layer containing equal concentrations of the hole transport layer (HTL) and electron transport layer (ETL) materials (host molecules) and 4 mol% of emitter molecules (guest). The energy level structure is shown in **Figure 3**a, and the simulation parameters as given in Table 1 are used. The shallow LUMO and deep HOMO energies of the HTL and ETL, respectively, ensure perfect carrier blocking, so the recombination efficiency is 100%. We already showed for similar single-matrix OLEDs that the carefully chosen guest trap depth (0.2 eV for electrons and holes) leads to a quite optimal balance between a small roll-off and a low operating voltage.[5] First, the OLED performance under steady-state conditions (no degradation) is discussed (Figures 3b–e). Subsequently, the decrease of the emission in the presence of degradation is shown (Figure 3f).

Figure 3b shows the roll-off of the IQE as a function of the current density and (inset) the current–voltage ($J(V)$) curve in the range 3–6 V. The full curve is a fit to the roll-off using the often-used empirical expression

$$\eta_{IQE} = \frac{\eta_{rad}}{1+\left(\frac{J}{J_{50}}\right)^{m}} \tag{4}$$

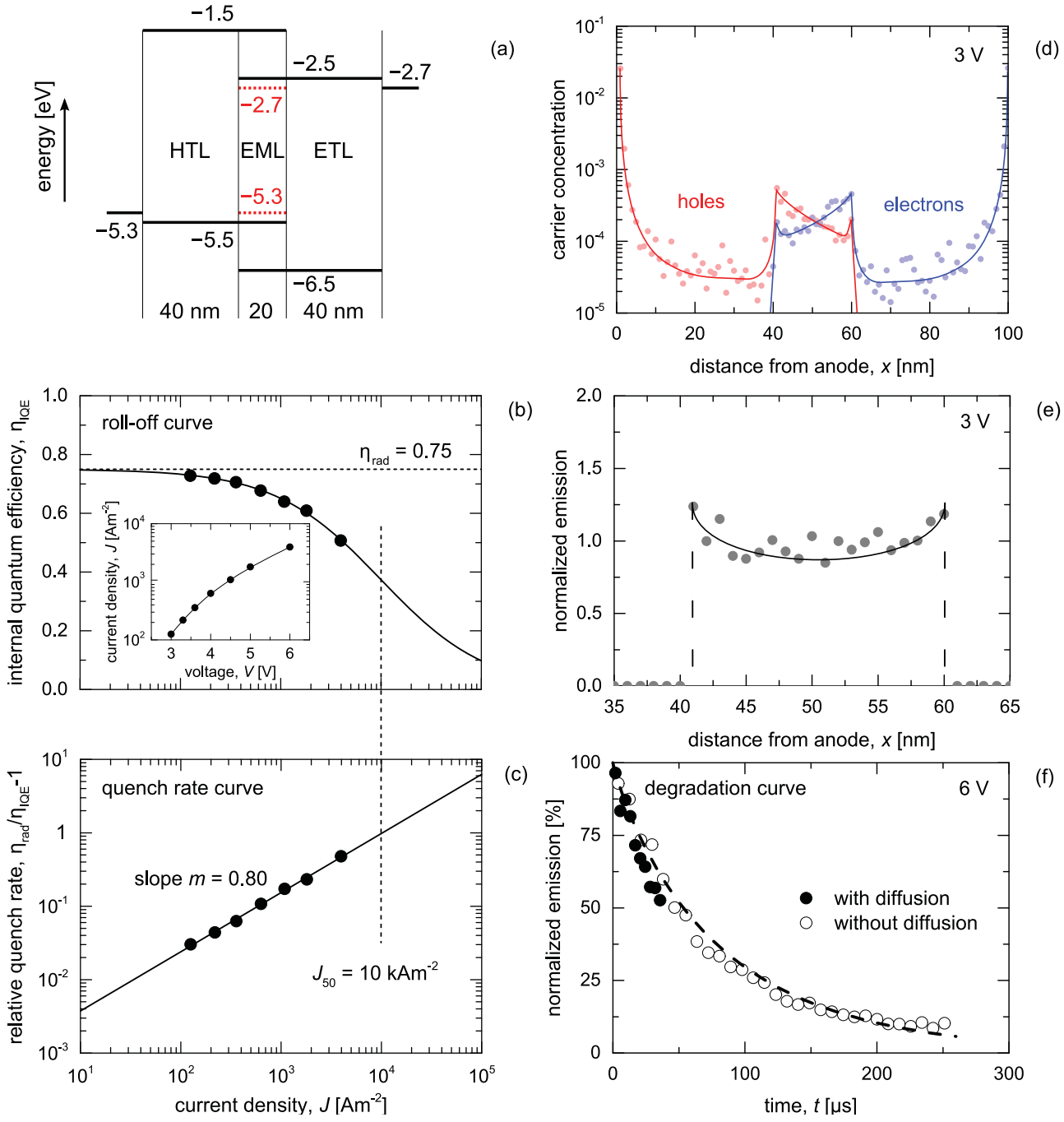

Figure 3. 3D-KMC simulation example, as discussed in Section 2.5. a) Energy level structure of the OLED considered. b) Current density dependence of internal quantum efficiency. The full curve is a fit using Equation (4). c) Current density dependence of the relative quench rate. d) Hole and electron concentration profiles at 3 V. The full curves are guides-to-the-eye. The molecular layers in the EML are at a distance of 41 to 60 nm from the anode, and the cathode is at a distance of 101 nm from the anode. e) Emission profile at 3 V. The full curve is a guide-to-the-eye. f) Time-dependence of the normalized emission at 6 V (degradation study), assuming only TPQ-t processes and assuming $p_{degr} = 1$, with and without exciton diffusion (closed and open symbols, respectively). The dashed curve is a stretched-exponential fit to the simulation results without diffusion, using the parameter values discussed in the text. In (b,c) the statistical uncertainty of the data points is smaller than the size of the data points. In (d–f) the statistical uncertainty may be judged from the variability with the position and time, respectively.

with J_{50} the current density at which the IQE has been reduced by a factor 2, and m an exponent which increases with increasing steepness of the roll-off around J_{50}. It may be seen that this expression provides an excellent fit. Alternatively, the IQE may be written as $\eta_{IQE} = [\Gamma/(\Gamma + \Gamma_q)]\eta_{rad}$, with Γ_q the effective rate of all loss processes due to quenching (and annihilation).

It follows from Equation (4) that the relative quench rate, Γ_q/Γ, may be expressed as

$$\frac{\Gamma_q}{\Gamma} = \frac{\eta_{rad}}{\eta_{IQE}} - 1 = \left(\frac{J}{J_{50}}\right)^m \quad (5)$$

A double logarithmic plot of the quantity $[(\eta_{rad}/\eta_{IQE}) - 1]$ should then yield a straight line with a slope m and an x-axis zero-crossing at $J = J_{50}$. We call this a "quench rate plot". Possible deviations from Equation (4) for small current densities can be seen more clearly from such a plot than from the roll-off curve. Figure 3c shows that Equation (4) is indeed well obeyed within the current density range studied. The fit parameters are $J_{50} = 10.0$ kA/m^2 and $m = 0.80$. Such a fit makes it possible to quite accurately derive the roll-off at small current densities, where the simulation results are somewhat less accurate due to relatively larger statistical fluctuations. The current density $J_{90} = (1/9)^{1/m} J_{50}$, which is a more commonly used measure for the roll-off,[12] is equal to 642 A/m^2. This value is higher than the highest values of J_{90} for phosphorescent OLEDs reported to date, which range up to 300 A/m^2.[12] We attribute the improved roll-off in the simulated device to the effect of carrier trapping on the mobility in the EML. Figure 3d,e shows the charge carrier concentration and emission profiles, respectively, at 3 V. As may be seen from the figures, strong accumulation of electrons at the anode-side of the EML and of holes at the cathode-side of the EML is prevented, and the emission profile is quite uniform across the thickness of the EML. A study in Section 4 of the effect of the guest trap depth supports this picture. We find that in the current density range studied the roll-off is almost completely due to TPQ. We found a similar conclusion for $Ir(ppy)_3$ and PtOEP based devices, where the small contribution of TTA was attributed to the relatively small triplet concentration in the devices at the current densities studied.[5]

Figure 3f shows for the same device the decrease of the emission at 6 V as a function of the time during a degradation simulation, assuming only TPQ-t processes and for $p_{degr} = 1$. The excited polaron is then in all cases located on the dye molecule, so that each TPQ process leads to degradation of the dye site involved. The simulations were carried out with and without triplet exciton diffusion. Switching off diffusion makes the simulations computationally less intensive, so that for the same total simulation (CPU) time the simulated time is much larger. Under these strongly accelerated conditions, the time at which the emission is reduced to 90% of the $t = 0$ value (LT90) is (5.5 ± 1.0) and (7 ± 2) µs, respectively. For the small emitter concentration used, the effect of diffusion of excitons to already degraded sites is thus quite small. The figure shows that a stretched exponential function (dashed curve, $I \propto \exp[-(t/\tau_{life})\,\beta)$ with a (1/e) lifetime $\tau_{life} \approx 80$ µs and $\beta \approx 0.91$) provides a reasonable, although not perfect, fit. In Section 4 we show that diffusion becomes more important at larger dye concentrations. Simulations of this type are expected to provide a prediction of the real lifetime for any other dye concentration and EML thickness after extrapolation of the simulation results to smaller current densities, and after a "calibration" experiment to deduce the actual value of p_{degr}.

3. The Uniform Density Model—The Relationship Between Roll-Off and Lifetime

In this section, it is first shown how within the framework of the uniform density model (UDM) simplified expressions may be obtained for the dependence of the IQE roll-off on the material and device parameters (subsection 3.1). The analysis leads to a shape of the roll-off curves which is consistent with the empirical roll-off given in Equation (4), and obtained from the 3D-KMC simulations shown in Figure 3. In subsection 3.2, it is shown how, under the assumption that upon a triplet-polaron quenching process subsequently (with a small probability) a degradation process takes place, the lifetime is related to material and device parameters. The analysis suggests that the exponent which gives the superlinear decrease of the lifetime with increasing current density in an accelerated lifetime experiment may be obtained from the shape of the roll-off curve. In Sections 4 and 5, the predictions from the model will be compared to simulation results for various OLED layer structures.

3.1. Roll-Off

Within the TPQ-related degradation mechanisms considered in this paper, the roll-off and lifetime are related. Even if for certain operational conditions the IQE loss due to TPQ is small, it will thus be of interest to understand how it depends on the material parameters. In general, the electron, hole and exciton densities show a dependence on the position in the EML, precluding the development of an analytical model for the efficiency roll-off. However, we find that it is nevertheless useful to further develop a simplified model within which the carrier density non-uniformity across the EML or across the part of the EML within which the emission takes place ("emission zone") is neglected.[11,12] Within this uniform density model, an OLED is regarded as a "chemical reaction vessel", with "reactants" (electrons and holes) and "products" (excitons). The interactions between all these species can be complex, but the neglect of a spatial dependence strongly simplifies the analysis. Figure 3e shows that it is indeed possible to obtain under some conditions a quite uniform emission profile in the EML. In this section, we extend the UDM by including the effect of a charge-carrier density of the mobility and diffusion coefficient, and by including a mechanistic description of the TPQ rate, leading to a refined expression for the roll-off.

We consider a phosphorescent OLED with in the emission zone uniform and equal electron and hole volume densities, $n_e = n_h = n$, and a uniform triplet density, n_T. Under steady-state conditions, the exciton generation rate is equal to the exciton loss rates due to radiative and non-radiative decay, TPQ, TTA and dissociation. Neglecting TTA (as the simulations shown in Section 2.5 and shown by van Eersel et al.[5] suggest that TPQ is more relevant) and dissociation, the triplet density balance may under steady-state conditions be written as

$$\frac{dn_T}{dt} = -\frac{n_T}{\tau} - 2k_{TPQ} n n_T + \frac{2e}{\varepsilon} n^2 \mu(n) = 0 \quad (6)$$

with k_{TPQ} the TPQ rate coefficient, $\mu(n)$ the charge density dependent mobility, which is assumed to be equal for holes and electrons, and with the last (generation) term as expected from the Langevin formula, neglecting the electric field dependence of the exciton generation rate and neglecting a correction to the mobility in bipolar devices.[36] The radiative decay rate will be proportional to the triplet density, so that from Equation (6) the IQE roll-off is given by

$$\eta_{IQE}(J) = \frac{n_T}{n_T(k_{TPQ}=0)}\eta_{rad} = \frac{\eta_{rad}}{1+2\tau k_{TPQ} n} \tag{7}$$

Simple expressions for the current density dependent functions $n(J)$ and $k_{TPQ}(J)$ may be obtained as follows. The condition of charge conservation (the number of injected carriers is equal to the number of excitons created, both per unit of time and area) implies that

$$\frac{J}{e} = \frac{e}{\varepsilon} 2n^2 \mu(n) \times d \tag{8}$$

with d the thickness of the recombination zone (or, for a well-designed OLED, the thickness of the EML). We assume that the mobility may be expressed as

$$\mu(n) \cong \mu_1 \left(\frac{n}{N_t}\right)^b \tag{9}$$

where the prefactor μ_1 is the mobility as obtained by extrapolation from the carrier density range of interest to the total site density, N_t (i.e., at a carrier concentration $c \equiv n/N_t$ equal to 1), and with $b > 0$. The electric field dependence of the mobility has been neglected. Equation (9) is exact for the case of an exponential density of states (DOS),[37] and provides for a Gaussian DOS a fair approximation in charge carrier density ranges with a width of at least one order of magnitude.[29] In both cases, b increases with increasing energetic disorder. An effective carrier density dependence of the mobility arises also in host-guest systems with a bimodal Gaussian density of states.[38] The exponent b depends then on the energy distance between the host and guest states. Combining Equations (8) and (9) leads to

$$n = \left(\frac{\varepsilon N_t^b}{2e^2 d \mu_1} J\right)^{\frac{1}{2+b}} \tag{10}$$

Note that n does not depend on the triplet-polaron quench rate. Triplet-polaron quenching is the result of encounters of diffusing triplets and polarons. In phosphorescent OLEDs, with typical dye concentrations of 5–10 mol%, the diffusion length of triplets is very small (of the order of the Förster radius, which we take 1.5 nm). TPQ is therefore predominantly due to the diffusion of the charge carriers, so that k_{TPQ} is proportional to the charge carrier diffusion coefficient, D. From diffusion theory,[39] it is known that for the case of a capture radius R_c, the rate coefficient is then given by

$$k_{TPQ}(n) = 4\pi D(n) R_c = 4\pi \frac{k_B T}{e} \mu(n) R_c \tag{11}$$

where the second step has been made using the Einstein equation which relates the diffusion coefficient to the mobility. The TPQ rate coefficient is thus carrier density dependent. The electric field dependence of the diffusion coefficient has been neglected. For simplicity, we have used the standard form of the Einstein equation, for non-interacting particles, instead of the generalized Einstein equation which would lead to a correction at high carrier densities.[40] From Equation (7–11) it follows that

$$\eta_{IQE}(J) = \frac{\eta_{rad}}{1+8\pi \frac{k_B T}{e} R_c \tau \left(\frac{\mu_1}{N_t}\right)^{\frac{1}{2+b}} \left(\frac{\varepsilon}{2e^2 d} J\right)^{\frac{1+b}{2+b}}} \tag{12}$$

This simplified analysis leads thus to expression for the roll-off which is consistent with the empirical expression (Equation 4) which is often found experimentally in OLEDs. Also the roll-off as obtained from simulations for the devices studied in this paper is quite well described using Equation 4 (see Section 2.5 and Section 4). The parameter values m and J_{50} are given in **Table 2** for the general case and for the specific case of a constant mobility ($b = 0$). If all other factors remain the same, the roll-off can thus be reduced by i) decreasing the mobility in the EML (as then the TPQ rate decreases), ii) increasing the emission zone thickness (as then the polaron density decreases), iii) decreasing the radiative decay time (as then radiative decay better outcompetes TPQ), and iv) reducing the TPQ capture radius.

The model suggests that the slope of the quench rate curve will be in the range 0.5 to 1.0, depending on the (effective) disorder of the mobility in the EML. The value $m = 0.80$ found for the example discussed in Section 2.5 is well in that range. The effective mobility exponent b is then approximately equal to 3. Interestingly, only a relatively weak sensitivity of the relative quench rate and J_{50} to the mobility prefactor μ_1 is then expected, viz. $\Gamma_q/\Gamma \propto \mu_1^{-0.2}$ and $J_{50} \propto \mu_1^{-0.25}$.

Table 2. Summary of roll-off parameters for the case of uniform and equal carrier densities, equal electron and hole mobility functions, equal exciton-polaron quench rates, and no dissociation. For the case $b = 0$, we have $\mu_1 = \mu$.

General case	Constant mobility ($b = 0$)
$m = \frac{1+b}{2+b}$	$m = \frac{1}{2}$
$J_{50} = \frac{2e^2 d}{\varepsilon \left(\frac{\mu_1}{N_t^b}\right)^{\frac{1}{1+b}} \left[8\pi \left(\frac{k_B T}{e}\right) R_c \tau\right]^{\frac{2+b}{1+b}}}$	$J_{50} = \frac{e^4 d}{\varepsilon \mu \times 32 (\pi k_B T R_c \tau)^2}$

3.2. Lifetime

Within the UDM, the degradation rate of an emitter molecule in the EML is given by

$$\frac{df_{degr}}{dt} = g \times p_q \times p_{qd} \times p_{degr} \times \left(1 - f_{degr}\right) \quad (13)$$

with $f_{degr}(t)$ the fraction of the emitter molecules which on time t has already degraded, p_q the probability that an exciton is lost due to TPQ, p_{qd} the probability that the TPQ process occurs on a dye site (which depends on the type of TPQ-process considered and on the emitter density, see Section 5), and p_{degr} the probability that an excited polaronic dye molecule degrades. The value of p_{degr} depends on the chemical stability of the molecule, and must be determined experimentally. Within the framework of the UDM, the exciton generation rate per dye site is equal to

$$g = \frac{J}{e \times d \times n_{dye}} \quad (14)$$

with n_{dye} the volume density of emitter molecules in the EML. If the light emission intensity $I(t)$ is proportional to the fraction of non-degraded sites, as expected in the absence of exciton diffusion, it is (from Equation (13)) given by

$$I(t) = \left(1 - f_{degr}\right) I(0) = \exp\left(-\frac{t}{\tau_{life,nd}}\right) I(0) \quad (15)$$

with a (1/e) lifetime when no exciton diffusion is included, $\tau_{life,nd}$, given by

$$\tau_{life,nd} = \frac{1}{p_q p_{qd} p_{degr}} \times \frac{e \times d \times n_{dye}}{J} \quad (16)$$

Using that $p_q = (1 - \eta_{IQE}/\eta_{rad})$, when writing $\eta_{IQE} = \eta_{rad}/[1+(J/J_{50})^m]$, where J_{50} and m can be obtained from Table 2, it follows that $p_q \cong (J/J_{50})^m$ for small current densities ($J << J_{50}$), so that then

$$\tau_{life,nd} \cong \frac{1}{p_{qd} p_{degr}} \times \frac{e \times d \times n_{dye} \times J_{50}^m}{J^{m+1}} \quad (17)$$

The model thus establishes a relationship between the roll-off and the lifetime in the absence of exciton diffusion. If valid, Equation (17) can be used to predict $\tau_{life,nd}$ already from a steady-state simulation, instead of from a usually computationally more demanding explicit 3D-KMC lifetime simulation. For the case of the systems discussed in Section 2.5, the dye concentration dependence of the lifetime predicted by Equation (17) will be investigated in Section 5.

Equation (17) furthermore leads to an algebraic dependence of the lifetime on the current density, $\tau_{life} \propto J^{-n}$, with a current density acceleration exponent $n = m + 1$. As m was predicted to fall in the range 0.5 to 1, n will be in the range 1.5 to 2. Such a current density dependence is indeed often observed in accelerated lifetime experiments.[41]

4. Sensitivity of the Roll-Off to Material Parameters

The benefits of using the symmetric mixed-matrix OLEDs of the type shown in Figure 3a are found to be quite similar to those of the otherwise identical single-matrix OLEDs studied by van Eersel et al.[5] Due to the use of dyes which act as hole and electron traps with a trap depth, Δ_1, around 0.2 eV, the carriers are slowed down in the EML, so that no charge accumulation occurs in the EML near the interfaces. At voltages around 3 V and below, the emission profiles are quite uniform, leading to a small IQE-loss. In this section we further analyze the sensitivity of the roll-off to Δ_1, to a hole (electron) injection barrier Δ_2 from the HTL to the host in the EML (from the ETL to the host in the EML), and to various other material parameters including the triplet emissive lifetime, triplet binding energy and the Förster radius for triplet diffusion. **Figure 4**a shows the energy level structure of the devices studied. The analysis leads to two energy level design rules from which the roll-off can be minimized without introducing a large voltage increase.

Figure 4b shows the quench rate curves for devices of the type shown in Figure 4a, with variable guest trap depths Δ_1 in the range 0–0.5 eV and with Δ_2 = 0 eV. The simulations were carried out for a series of voltages in the range 3–6 V, for the parameter values given in Table 1 and for a typical Ir-dye concentration of 4 mol%. Results for the case Δ_1 = 0.2 eV were already given in Figure 3. The figure confirms in a quantitative manner the more qualitative picture mentioned above. It may be seen that for all values of Δ_1, the empirical expression (Equation (4)) for the roll-off is well obeyed, with a value of J_0 which increases until it saturates for $\Delta_1 \cong$ 0.2 eV. The use of deeper traps leads to a significant reduction of the current density at a given voltage, and is therefore unfavorable from a point of view of optimizing the power efficiency. That may be seen from the current density at a fixed voltage, that is, 3 V and 4 V (indicated in the figures by large and filled symbols). We find that variations of i) the disorder energy σ, from 0.075 to 0.125 eV, ii) the EML layer thickness d, from 10 to 30 nm (at a fixed 100 nm total thickness), or iii) the wavefunction decay length λ (from 0.3 to 0.1 nm) have no significant or only little effect on this picture. For single-matrix OLEDs we find that for $\Delta_1 < 0.2$ eV the quench rate is a factor ≈1.5 larger than for the mixed-matrix devices, and that saturation occurs at $\Delta_1 \cong$ 0.25–0.3 eV; the quench rate curves coincide then to those shown in Figure 4b. We attribute this to the somewhat larger mobility in single-matrix OLEDs, as all host molecules contribute to the transport, so that deeper traps are needed to obtain a uniform emission profile. A first design rule for symmetric OLEDs is thus that the dye trap depth Δ_1 should ideally be ≈0.2 eV or 0.25–0.3 eV, for mixed-matrix or single-matrix OLEDs, respectively.

As a second design rule, we find that the HTL-EML(host) and ETL-EML(host) injection barriers Δ_2 should ideally be (0.0 ± 0.1) eV. This may be concluded from Figure 4c, which shows the effect of variations of Δ_2 from –0.3 to +0.3 eV, for a fixed value Δ_1 = 0.2 eV. For positive injection barriers, accumulation of charges occurs in the transport layers, which enhances the TPQ rate near the EML interfaces. When decreasing the barrier to $\Delta_2 \cong$ 0, the decrease of the relative quench rates saturates. Although a further reduction of Δ_2 does not further diminish the roll-off, it gives rise to an increase of the voltage required to obtain a certain current density, as dissipation occurs due to the energy loss when the carriers enter the EML.

Figure 4c shows that the quench rate at small current densities and the slope parameter m characterizing the relative

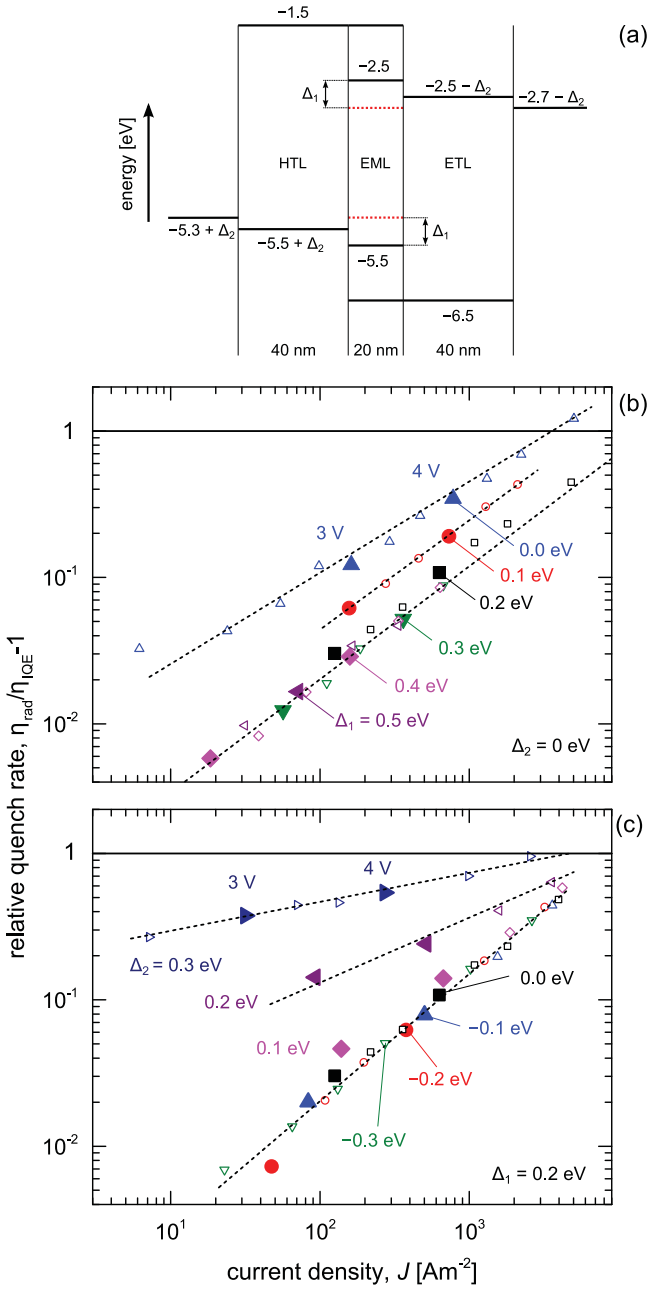

Figure 4. a) Energy level structure of the symmetric OLEDs studied. In the EML, a 50:50 mixture of two materials with a 4.0 eV single-particle energy gap is used. b) Quench rate curves for OLEDs as show in (a), with a varying energy distance Δ_1 between the host and guest levels in the EML and with $\Delta_2 = 0$ eV. The results shown in the figure provide a motivation for the first OLEDs design rule, discussed in Section 4. c) Quench rate curves for OLEDs as shown in (a), with fixed energy levels in the EML ($\Delta_1 = 0.2$ eV), but with varying barrier heights Δ_2 from the HTL and the ETL to the host levels in the EML. The $\Delta_2 = 0.0$ eV case is as shown in Figure 3. The results shown in the figure provide a motivation for the second OLEDs design rule, discussed in Section 4. In both figures, large and filled symbols indicate the data points obtained at 3 and 4 V. The statistical uncertainty of the data points is for $J > 10^2$ A/m^2 of the order of the symbol sizes, as may be judged from a comparison with the linear dashed guides-to-the-eye, but becomes somewhat larger for smaller current densities.

quench rate curves do not only depend on the transport and excitonic parameters in the EML, but also on the injection boundary conditions. We find that their effect on the shape of the emission profiles, and thereby on the roll-off, cannot be neglected. Giving a detailed quantitative analysis is beyond the scope of this paper; we limit ourselves here to a brief qualitative discussion. In the absence of injection barriers ($\Delta_2 \leq 0$ eV), the emission profiles for systems with $\Delta_1 \geq 0.2$ eV are found to be quite uniform at low voltages. However, above 3 V, only part of the exciton generation occurs in the bulk of the EML. A fraction of the charges passes the EML and is finally blocked. Charge accumulation zones develop near the EML interfaces, and the emission originates to an increasing extent from these interfacial zones. The gradual splitting of the emission profile into two narrow peaks near the interfaces is expected to contribute to the large slope of the relative quench rate curves. Using Equation (10), we deduce for such devices a value of $b \cong 1.33$ from an analysis of the carrier density dependence of the current density in the center of the EML (where due to the symmetry the electron and hole densities are equal). Within the framework of the UDM, this value would lead to $m \cong 0.7$, which is indeed somewhat smaller than the value $m \cong 0.80$ obtained from the quench rate curves. In the presence of large barriers for carrier injection into the EML ($\Delta_2 \geq 0.2$ eV), charge accumulation occurs already at small voltages near the EML interfaces. The emission is then almost completely confined to the two thin interfacial zones. As a result of the large local carrier density, TPQ leads already at low current densities to a relatively large quench rate. With increasing voltage (and current density), the effect of the injection barriers at the EML interfaces is reduced. There is then less charge accumulation near the interfaces, and a larger fraction of the exciton formation occurs in the bulk of the EML, where the charge density is relatively small. These two effects explain the small slope of the relative quench rate curve for such cases, for example, $m \cong 0.20$ for devices with $\Delta_2 = 0.3$ eV (as may be deduced from Figure 4c).

As a next step, we have investigated the sensitivity of the roll-off to a variation of the hopping attempt rate to the first neighbor, ν_1, throughout the entire device. This corresponds to a variation of the mobility prefactor μ_1 introduced in Section 3. The simulations confirm the expectation that for the symmetric devices studied the relative quench rate curves are only weakly sensitive to μ_1. For simulations with ν_1 enhanced or decreased by a factor of 100 as compared to the value given in Table 1, the relative quench rates as extrapolated to $J = 10$ A/m^2 are found to differ by only a factor ≈5.[42] From Equation (12), a factor ≈6.3 would be expected when assuming the value $b = 3.0$ which would follow from the observed slope parameter $m = 0.80$. At larger current densities an even smaller effect of changing ν_1 was found; the J_0-values were only different by a factor ≈2. We emphasize that this result does not imply that the hopping attempt rates are not important to the roll-off of OLEDs. Layer-specific or charge carrier-specific differences, for example, may result in a non-uniform emission profile and hence in an increased efficiency loss.

Figure 5a,b show the sensitivity of the quench rate curves to the effective radiative decay time τ, at a fixed value of the radiative decay efficiency ($\eta_{rad} = 0.75$), for a triplet exciton binding energy, $E_{T,b}$, equal to 1.0 and 0.5 eV, respectively. Simulation

results for 0.75 eV (not shown) are essentially the same as for 1.0 eV. As mentioned in Section 2.4, a significant dissociation rate is expected unless $E_{T,b}$ is well above $E_{CT,b}$ = 0.48 eV. This is confirmed by simulation results. If $E_{T,b}$ is 0.75 eV or higher, the quenching loss is essentially independent of $E_{T,b}$. Furthermore, it is simply inversely proportional to τ (dashed lines) as expected from Equation (12). The roll-off is sensitive to $E_{T,b}$ below a value of 0.75 eV, as may be seen from the $J_{50}(E_{T,b})$ dependence shown in **Figure 6** (closed symbols). For $E_{T,b}$ = 0.5 eV, the quench rate is significantly enhanced, in particular at small current densities, so that the roll-off curves do not obey Equation (4) anymore. The observed reduction of the slope of the quench rate curves, to values which can be smaller then 0.5, may be understood from an extension of the UDM which includes dissociation.[42] The observation that at very large current densities the effect of dissociation becomes less may be explained by considering that then such a high volume density of charge carriers is available for exciton formation that very soon after dissociation already new pairs are formed.

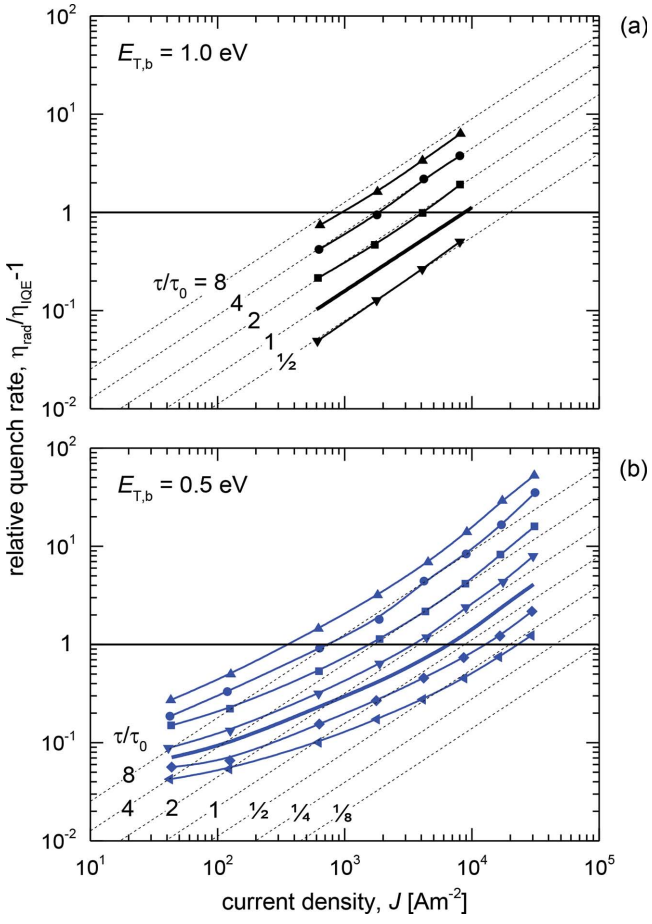

Figure 5. Current density dependence of the relative quench rate for OLEDs as shown in Figure 3a for various effective radiative decay times relative to the default value (τ_0 = 1.38 µs, see Table 1), for a) $E_{T,b}$ = 1.0 eV, and b) $E_{T,b}$ = 0.5 eV. Thick curves indicate the results for $\tau = \tau_0$, and dashed lines indicate the linear τ/τ_0 dependence which is expected in the absence of dissociation, and using the $E_{T,b}$ = 1.0 eV result as a reference. The statistical uncertainty of the data points is of the order of the symbol sizes, or smaller.

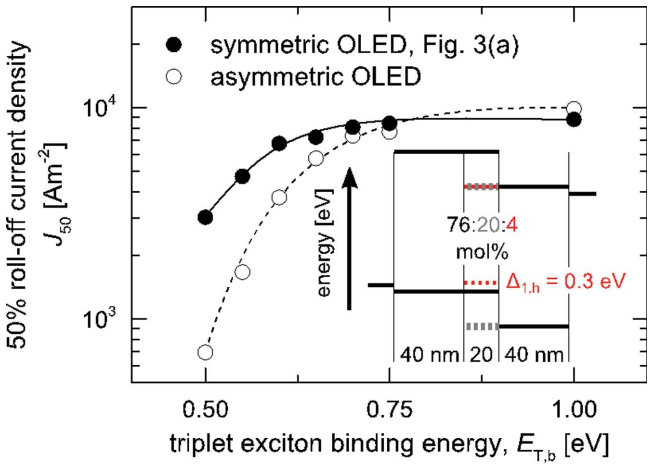

Figure 6. Closed circles: dependence of the 50% roll-off current density, J_{50}, on the triplet exciton binding energy, for symmetric mixed-matrix OLEDs with an energy level structure as given in Figure 3a (closed symbols). Open circles: J_{50} for asymmetric mixed OLEDs with the same HTL, EML (host), and ETL energy level structure, but with a guest HOMO and LUMO level structure as shown in the inset and with in the EML a composition as indicated. The statistical uncertainty of the data points is of the order of the symbol size.

At the 4 mol% dye concentration assumed in the preceding simulations, and for the small Förster radius for triplet diffusion assumed ($R_{F,diff}$ = 1.5 nm), triplet diffusion does not contribute significantly to the TPQ rate. In **Figure 7**, the results of a study of the role of triplet diffusion are shown. For clarity, Dexter-type diffusion has been switched off. Varying $R_{F,diff}$ in steps of 1.5 nm reveals only a significant contribution to the roll-off for $R_{F,diff}$ equal to 3 nm and larger, for the default 4 mol% dye concentration as well as for 8 mol% devices. The figure also shows that increasing the dye concentration increases the sensitivity to triplet diffusion, as expected. The effect of triplet diffusion is largest at small current densities, so that the quench rate curves become nonlinear, as due to the carrier density dependence of the polaron diffusion coefficient the relative role of polaron diffusion is larger at large current densities. We conclude that for dye concentrations of 8 mol% or less, the uncertainty concerning the most appropriate description of triplet diffusion is expected to contribute only a small uncertainty to the simulation results presented above. We note that triplet diffusion can also contribute to less roll-off, viz. when in the case of a strongly nonuniform emission profile the triplets migrate to regions with a smaller polaron density.[43]

Realizing OLEDs which satisfy the first design rule (equal ≈0.2 eV hole and electron trap depths due to the guest levels in the EML) is in practice not always well possible, due to a lack of suitable host materials with accurately tuned HOMO and LUMO levels. It is therefore of interest to investigate the sensitivity to deviations of the precise relative positions of the host and guest energy levels. The open circles in Figure 5 show the results of such a study, carried out for asymmetric mixed-matrix OLEDs with $\Delta_{1,h}$ = 0.3 eV hole trap depth and a $\Delta_{1,e}$ = 0 eV electron trap depth (as shown in the inset). By choosing unequal concentrations of the hole and electron transporting

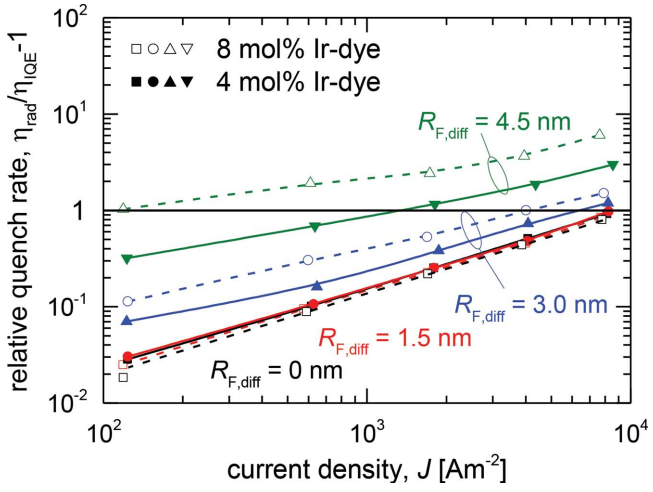

Figure 7. Dependence of the quenching curves on the Förster radius for triplet exciton diffusion, $R_{F,diff}$, for two values of the Ir-dye concentration, obtained from simulations for the OLED shown in Figure 3a. The full and dashed curves are guides-to-the-eye, consistent with the numerical accuracy of the simulation data. The statistical uncertainty of the data points is equal to symbol sizes, or smaller, except for the data points close to $J = 10^2$ A/m^2, where it is slightly larger.

host materials in the EML (76 and 20 mol%, respectively), the reduction of the effective hole mobility due to the trapping of holes at dye sites is partially compensated. The simulation results show a much stronger sensitivity of the roll-off to $E_{T,b}$ than for the case of a symmetric OLED with $\Delta_{1,h} = \Delta_{1,e} = 0.2$ eV (closed spheres). This may be attributed to the strongly enhanced triplet exciton dissociation probability, as also CT states consisting of a hole on a dye site and an electron on a host site can be formed.

In view of the sensitivity of the roll-off to $E_{T,b}$, it is important to be able to obtain its value accurately from experiment. By definition, $E_{T,b} = E_{LUMO} - E_{HOMO} - E_T$. It can therefore be obtained, at least in principle, from a determination of the single particle energy gap, $E_{LUMO} - E_{HOMO}$, and a measurement of the triplet energy. However, the accuracy of commonly used methods for obtaining E_{HOMO} and E_{LUMO} from e.g., cyclic voltammetry, from a combination of photoelectron spectroscopy and inverse photoelectron spectroscopy, or from density functional theory calculations, is a subject of current debate.[5,44,45] Partial information follows from the difference between the singlet and triplet exciton energies, which for the commonly used green emitter material Ir(ppy)$_3$ is approximately 0.4 eV.[46] Assuming a singlet exciton binding energy of a few tenths of an eV, $E_{T,b}$ would then be around 0.6–0.9 eV.

5. Sensitivity of the OLED Lifetime to the Ir-Dye Concentration

In this section, a comparison is given between the results of explicit 3D-KMC simulations of the lifetime of OLEDs of the type shown in Figure 3a, for a range of Ir-dye concentrations, and the prediction obtained from the UDM discussed in Section 4. When exciton diffusion may be neglected, a fair agreement is obtained for the TPQ-p and TPQ-t degradation scenarios. From a comparison of the simulated lifetimes with the experimental lifetime in state-of-the-art devices, an estimate is made of the degradation probability per TPQ process, p_{degr}.

Figure 8 shows the results of 3D-KMC simulations of the lifetime of OLEDs of the type shown in Figure 3a as a function of the Ir-dye concentration in the EML, at a fixed voltage (6 V), for the case of TPQ-p and TPQ-t processes (see Figure 2). The simulations were carried out with the purpose to investigate the usefulness of the UDM as a means to predict the OLED lifetime from the results of steady-state simulations, and to investigate to what extent exciton diffusion (which was neglected in the UDM) affects the results. Typical examples of the raw simulation data were already shown in Figure 2f.

In the case of a TPQ-t process, the excited-state polaron is created on the molecule where the exciton was located. With a very high probability, around 0.97 and 0.98 for Ir-dye concentrations $x_{Ir} = 2$ and 4 mol%, respectively, and for higher concentrations essentially 1, the excitons are located on the dye sites. Each TPQ process then leads to the conversion of an emissive dye molecule into a degraded (non-emissive) dye molecule, so that $p_{qd} \cong 1$ in Equation (17). It follows from Equation (17) that the lifetime is then expected to be proportional to the volume density of Ir-dye molecules, if all other factors remain constant. However, the actual concentration dependence is affected by the concentration dependence of the current density, which is found to be minimal around $x_{Ir} \cong 9$ mol%. At smaller concentrations, the dyes act predominantly as trap sites, so that the mobility then decreases with increasing x_{Ir}, whereas at larger concentrations direct dye-dye transport is the predominant transport mechanism. The mobility then increases with increasing x_{Ir}. Figure 8 (closed spheres) shows that the predicted LT90 lifetime indeed increases for small x_{Ir}, but that it shows a maximum around 15 mol%. The lifetime as obtained from explicit 3D-KMC simulations is for small dye concentrations within a factor 2 of the predicted value, but is smaller by a factor of approximately 4 for large concentrations. The difference at large dye concentrations is mainly due to the neglect of exciton diffusion in the UDM, as may be concluded from the observation that simulations within which diffusion is switched off (small circles) agree then excellently with the prediction from the UDM. The small discrepancy at small concentrations might be due to deviations from a uniform emission profile, either laterally or in the direction perpendicular to the EML.

Upon a TPQ-p process, the excited-state polaron is created on the molecule at which the polaron was located. From the steady-state simulations, we find that the probability that TPQ occurs on a dye site (p_{qd}) is to an excellent approximation proportional to x_{Ir}, and approximately 0.42 for $x_{Ir} = 0.1$. As a result, the lifetime as predicted from Equation (17) is approximately independent of x_{Ir} (closed squares in Figure 8), and larger than as expected for the TPQ-t scenario. The explicit 3D-KMC simulation results (open squares) confirm the latter expectation. However, the x_{Ir} dependence is larger than expected. A preliminary analysis suggests that the statistics of the occurrence of emitter pairs strongly affects the lifetime for this case. As degradation only occurs when the exciton and polaron reside both on a dye molecule, it is for very small x_{Ir} rarer than would follow from continuum statistics. That explains the higher than expected lifetime for the 2 mol%

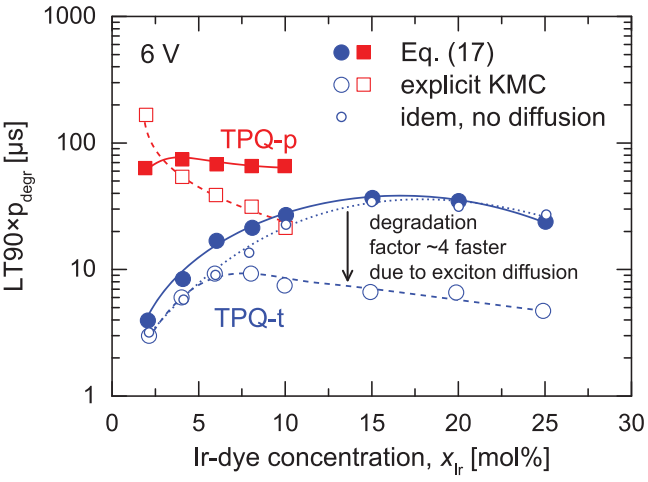

Figure 8. Results of explicit 3D-KMC lifetime for the OLEDs shown in Figure 3a (open symbols) as a function of the Ir-dye concentration, at 6 V, assuming TPQ-p processes (the triplet exciton hops to the site on which the polaron resides, open squares) or TPQ-t processes (the polaron hops to the site on which the triplet exciton resides, open circles). For the latter case, also simulation results without diffusion are included (small circles). The closed symbols give the predictions from the uniform density model (Equation (17)). The vertical scale gives the actual LT90 device lifetime, multiplied by the (very small) probability p_{degr} that upon a TPQ process degradation takes place. The results were obtained with p_{degr} = 1. The curves are guides-to-the-eye. The statistical uncertainty of the data points is equal to symbol sizes, or smaller.

case, and the observation of saturation of the degradation, viz. when each cluster of Ir-dye molecules contains a degraded molecule. The emission occurs then from the isolated dye molecules. Giving more in-depth analyses for both scenarios is beyond the scope of this paper.

The LT90 lifetime obtained from the simulations is in the range 5–50 µs when taking p_{degr} = 1, and for x_{Ir} in the 5–10 mol% range. The current density at 6 V as obtained from the simulations is approximately 4000 A/m^2. In efficient stacked state-of-the-art white OLEDs operated at a luminance equal to 1000 cd/m^2, the current density is much smaller, around 10 A/m^2. Assuming a current density acceleration exponent equal to 1.8 (as expected from the analysis given in Section 3.2), an actual LT90 lifetime of 10,000 hours would then imply an average value p_{degr} of the order 10^{-8}. A method for deducing that probability from the observed luminance degradation versus time and from transient photoluminescence studies of degraded devices has been demonstrated by Giebink et al.[9] Interestingly, for the systems studied, with in the EML a typical blue-emitting Ir-dye molecule embedded in a 4,4′-bis(3-methylcarbazole-9-yl)-2,2′-biphenyl (mCBP) host, a similar degradation probability per triplet-polaron encounter was found, viz. roughly 2×10^{-9}.

We note that the validity of the assumption that the degradation probability p_{degr} is independent of the material composition and simulation parameters has yet to be proven. It is conceivable that protective mechanisms leading to fast de-excitation of the excited polarons depend on, for example, the dye concentration or the applied electric field. If needed, such mechanisms can be included in the 3D-KMC approach developed.

6. Summary, Conclusions, and Outlook

Results have been presented of three-dimensional kinetic Monte Carlo (3D-KMC) simulations of the degradation in phosphorescent OLEDs, based on scenarios in which the emissive dye molecules are converted to non-emissive molecules upon a triplet-polaron quenching (TPQ) process. For the simulation parameters assumed, TPQ processes provide the predominant contribution to the IQE roll-off with increasing current density. Therefore, the roll-off and lifetime are related. From a simplified model, assuming uniform charge carrier and exciton densities across the emissive layer (EML), an analytical expression for the roll-off has been obtained in terms of the materials parameters. Within the same approach, an expression has been obtained (Equation 17) from which the lifetime due to TPQ-induced degradation can be obtained from steady-state simulations. The model is found to provide a fair prediction of the Ir-dye concentration dependence of the lifetime in a model system, provided that exciton diffusion may be neglected.

The 3D-KMC model provides a means to investigate the sensitivity of the roll-off and lifetime to the physical processes assumed, to the materials-specific parameters and to the layer stack architecture. In this paper, we have explored some of these relationships, including the sensitivity to energy level values, the mobility, the triplet binding energy, the emissive lifetime, energetic disorder, the mobility and exciton diffusion. We have established how in idealized symmetric OLEDs the roll-off can be minimized by following design rules for the trap depths of the dyes in the EML and for the injection barriers from the transport layers to the EML. Furthermore, it was found that the roll-off is quite sensitive to the triplet exciton binding energy, $E_{T,b}$, if that would be smaller than 0.75 eV (i.e., within the framework of our formalism less than 0.25 eV above the binding energy of CT-excitons with the electron and hole on nearest neighbor sites).

It follows from our results that the development of more accurate methods for determining the HOMO and LUMO energy levels and $E_{T,b}$, with an accuracy better than 0.1–0.2 eV, would make the simulations more versatile. Furthermore, simulation-assisted OLED lifetime studies should be carried out in order to establish the degradation mechanism. The simulation results suggest that it would be of interest to vary in such a study the emitter concentration as a means to make a distinction between different degradation scenarios.

Acknowledgements

The authors would like to thank the Philips Research e-Science department for technical support. This research was supported by the Dutch nanotechnology program NanoNextNL.

Received: July 28, 2014
Revised: September 25, 2014
Published online: November 4, 2014

[1] S. Reineke, M. Thomschke, B. Lüssem, K. Leo, *Rev. Mod. Phys.* **2013**, *85*, 1245.

[2] R. Coehoorn, P. A. Bobbert, *Phys. Status Solidi A* **2012**, *209*, 2354.
[3] J. J. M. van der Holst, M. A. Uijttewaal, B. Ramachandhran, R. Coehoorn, P. A. Bobbert, G. A. de Wijs, R. A. de Groot, *Phys. Rev. B* **2009**, *79*, 085203.
[4] M. Mesta, M. Carvelli, R. J. de Vries, H. van Eersel, J. J. M. van der Holst, M. Schober, M. Furno, B. Lüssem, K. Leo, P. Loebl, R. Coehoorn, P. A. Bobbert, *Nat. Mater.* **2013**, *12*, 652.
[5] H. van Eersel, P. A. Bobbert, R. A. J. Janssen, R. Coehoorn, *Appl. Phys. Lett.* 2014, *105*, 143303.
[6] N. C. Giebink, S. R. Forrest, *Phys. Rev. B* **2008**, *77*, 235215.
[7] D. Y. Kondakov, In *Organic Electronics*; CRC Press, Taylor & Francis Group, Boca Raton **2009**, p 211.
[8] S. Schmidbauer, A. Hohenleutner, B. König, *Adv. Mater.* **2013**, *25*, 2114.
[9] N. C. Giebink, B. W. D'Andrade, M. S. Weaver, P. B. Mackenzie, J. J. Brown, M. E. Thompson, S. R. Forrest, *J. Appl. Phys.* **2008**, *103*, 044509.
[10] N. C. Giebink, B. W. D'Andrade, M. S. Weaver, J. J. Brown, S. R. Forrest, *J. Appl. Phys.* **2009**, *105*, 124514.
[11] M. A. Baldo, C. Adachi, S. R. Forrest, *Phys. Rev. B* **2000**, *62*, 10967.
[12] C. Murawski, K. Leo, M. C. Gather, *Adv. Mater.* **2013**, *25*, 6801.
[13] S. Reineke, G. Schwartz, K. Walzer, M. Falke, K. Leo, *Appl. Phys. Lett.* **2009**, *94*, 163305.
[14] F. Lindla, M. Boesing, C. Zimmermann, F. Jessen, P. van Gemmern, D. Bertram, D. Keiper, N. Meyer, M. Heuken, H. Kalisch, R. H. Jansen, *Appl. Phys. Lett.* **2009**, *95*, 213305.
[15] N. C. Erickson, R. J. Holmes, *Appl. Phys. Lett.* **2010**, *97*, 083308.
[16] S. Reineke, K. Walzer, K. Leo, *Phys. Rev. B* **2007**, *75*, 125328.
[17] H. van Eersel, P. A. Bobbert, R. Coehoorn, unpublished.
[18] C. Weichsel, L. Burtone, S. Reineke, S. I. Hintschich, M. C. Gather, K. Leo, B. Lüssem, *Phys. Rev. B* **2012**, *86*, 075204.
[19] T. D. Schmidt, D. S. Setz, M. Flämmich, J. Frischeisen, D. Michaelis, B. C. Krummacher, N. Danz, W. Brütting, *Appl. Phys. Lett.* **2011**, *99*, 163302.
[20] W. C. Germs, J. J. M. van der Holst, S. L. M. van Mensfoort, P. A. Bobbert, R. Coehoorn, *Phys. Rev. B* **2011**, *84*, 165210.
[21] M. Mesta, J. Cottaar, R. Coehoorn, P. A. Bobbert, *Appl. Phys. Lett.* **2014**, *104*, 213301.
[22] A. Massé, R. Coehoorn, P. A. Bobbert, *Phys. Rev. Lett.* 2014, *113*, 116604.
[23] S. L. M. van Mensfoort, S. I. E. Vulto, R. A. J. Janssen, R. Coehoorn, *Phys. Rev. B* **2008**, *78*, 085208.
[24] O. Rubel, S. D. Baranovskii, P. Thomas, S. Yamasaki, *Phys. Rev. B* **2004**, *69*, 014206.
[25] H. T. Nicolai, A. J. Hof, M. Lu, P. W. M. Blom, R. J. de Vries, R. Coehoorn, *Appl. Phys. Lett.* **2011**, *99*, 203303.
[26] S. L. M. van Mensfoort, V. Shabro, R. J. de Vries, R. A. J. Janssen, R. Coehoorn, *J. Appl. Phys.* **2010**, *107*, 113710.
[27] M. Schober, M. Anderson, M. Thomschke, J. Widmer, M. Furno, R. Scholz, B. Lüssem, K. Leo, *Phys. Rev. B* **2011**, *84*, 165326.
[28] H. Bässler, *Phys. Status Solidi B* **1993**, *175*, 15.
[29] W. F. Pasveer, J. Cottaar, C. Tanase, R. Coehoorn, P. A. Bobbert, P. W. M. Blom, D. M. de Leeuw, M. A. J. Michels, *Phys. Rev. Lett.* **2005**, *94*, 206601.
[30] V. Coropceanu, J. Cornil, D. A. da Silva Filho, Y. Olivier, R. Silbey, J.-L. Brédas, *Chem. Rev.* **2007**, *107*, 926.
[31] J. Cottaar, L. J. A. Koster, R. Coehoorn, P. A. Bobbert, *Phys. Rev. Lett.* **2011**, *107*, 136601.
[32] Y. Kawamura, J. Brooks, J. J. Brown, H. Sasabe, C. Adachi, *Phys. Rev. Lett.* **2006**, *96*, 017404.
[33] E. B. Namdas, A. Ruseckas, I. D. W. Samuel, S.-C. Lo, P. L. Burn, *Appl. Phys. Lett.* **2005**, *86*, 091104.
[34] J. C. Ribierre, A. Ruseckas, K. Knights, S. V. Staton, N. Cumpstey, P. L. Burn, I. D. W. Samuel, *Phys. Rev. Lett.* **2008**, *100*, 017402.
[35] H. van Eersel, R. A. J. Janssen, P. A. Bobbert, R. Coehoorn, unpublished.
[36] J. J. M. van der Holst, F. W. A. van Oost, R. Coehoorn, P. A. Bobbert, *Phys. Rev. B* **2009**, *80*, 235202.
[37] M. C. J. M. Vissenberg, M. Matters, *Phys. Rev. B* **1998**, *57*, 12964.
[38] R. Coehoorn, *Phys. Rev. B* **2007**, *75*, 155203.
[39] S. Chandrasekhar, *Rev. Mod. Phys.* **1943**, *15*, 1.
[40] Y. Roichman, N. Tessler, *Appl. Phys. Lett.* **2002**, *80*, 1948.
[41] C. Kristukat, T. Gerloff, M. Hoffmann, K. Diekmann, In *Organic Light-Emitting Diodes (OLEDs): materials, devices and applications, Ch. 20,* (Ed: A. Buckley), Woodhead Publishing, Cambridge, UK **2013**.
[42] These simulations were carried out under the condition of zero exciton diffusion, in order to allow a proper comparison with the roll-off as obtained from the UDM.
[43] G. He, M. Pfeiffer, K. Leo, M. Hofmann, J. Birnstock, R. Pudzich, J. Salbeck, *Appl. Phys. Lett.* **2004**, *85*, 3911.
[44] B. W. D'Andrade, S. Datta, S. R. Forrest, P. Djurovich, E. Polikarpov, M. E. Thompson, *Org. Electron.* **2005**, *6*, 11.
[45] P. I. Djurovich, E. I. Mayo, S. R. Forrest, M. E. Thompson, *Org. Electron.* **2009**, *10*, 515.
[46] T. Tsuboi, *J. Lumin.* **2006**, *119–120*, 288.